Applied Radiation and Isotopes 72 (2013) 182–194

Contents lists available at SciVerse ScienceDirect

Applied Radiation and Isotopes

journal homepage: www.elsevier.com/locate/apradiso

Out-of-field beam characteristics of a 6 MV photon beam: Results of a Monte Carlo study

M. Atarod [a], P. Shokrani [a,*], A. Azarnoosh [b]

[a] Medical Physics Department, Isfahan University of Medical Sciences, Isfahan, Iran
[b] Physics Department, Islamic Azad University, Dezful Branch, Dezful, Iran

HIGHLIGHTS

- A Monte Carlo model of a 6 MV photon beam was created and verified.
- The spatial and energy distributions were determined in and out of the modeled beam.
- Variation of the evaluated beam characteristics with field size and depth was investigated.
- The contribution of internal scatter to peripheral radiation at different depths was determined.
- The out of field energy distributions were used to analyze out of field dosimetry factors.

ARTICLE INFO

Article history:
Received 3 July 2012
Received in revised form
5 October 2012
Accepted 17 October 2012
Available online 9 November 2012

Keywords:
Fluence
Photon
Monte Carlo
Out-of-field dose

ABSTRACT

Detailed characteristics of particles in the periphery of a 6 MV photon beam resulting from the exposure of a water phantom were analyzed. The characteristics at the periphery were determined with respect to particles' origin and charge, using Monte Carlo simulations. Results showed that in the peripheral regions, the energy fluence and the mean energy distribution of particles are independent of depth, and the majority of charged particles originate in the irradiated volume. The results are used to examine out-of-field dosimetry factors.

1. Introduction

In external beam radiotherapy, knowledge of the radiation dose in out-of-field regions, the so called peripheral dose (PD), is necessary in order to estimate the risk of secondary cancer, late tissue injuries and fetal abnormalities associated with radiation treatment. The PD is produced by photons originating from head leakage, scattering at accelerator components and scattering from irradiated region of the patient or phantom. The latter is identified as the patient or the phantom scatter component of PD. Reduction of this component is not possible by external shielding. Therefore, determination of this component of the PD may permit the reduction of the thickness of out-of-field shielding (Stoval et al., 1995). In order to determine the contribution of phantom scatter to PD, Monte Carlo simulations can be used to obtain the phase space information of photons and contaminant charged particles at different depths in a water phantom, inside and outside of the field's edge.

A number of Monte Carlo studies were performed in order to study the characteristics of clinical beams, such as planar fluence, angular distribution, the energy spectrum and the fractional contributions of treatment head components to PD (Mohan and Chui, 1985; Chaney and Cullip, 1994; Lovelock et al., 1995; Deng et al., 2000; Jiang et al., 2001; Ding, 2002; Kim et al., 2006; Chofor et al., 2010, 2012). In these studies, the importance of separating the extra-focal radiation (scattered photons from the primary collimator and the flattening filter) from the primary photons (photons directly from the target) for PD analysis of clinical photon beams was emphasized. However, previous analysis was performed mainly at the phantom surface or at a certain depth.

A number of experimental studies showed that, irrespective of energy, the PD is independent of depth (Stoval et al., 1995). In their Monte Carlo studies, Kry et al. (2006, 2007) reported that the out-of-field relative dose does not depend on depth, except for the buildup region where it increases substantially. On the contrary, Mohan and Chui (1985) showed by measurement that for a 15 MV photon, the

* Corresponding author. Tel.: +98 3117922411.
E-mail address: Shokrani@med.mui.ac.ir (P. Shokrani).

0969-8043/$ - see front matter © 2012 Elsevier Ltd. All rights reserved.
http://dx.doi.org/10.1016/j.apradiso.2012.10.013

peripheral percent depth dose (PDD) is similar to the PDD along the beam central axis, except for a 10% discrepancy outside of the buildup region. In summary, the characteristics of clinical beams such as planar fluence, angular distribution and mean energy spatial distribution were analyzed only at the phantom surface. Also, there is a lack of general agreement regarding the depth dependency of PD. Therefore, the goal of this study was to provide beam characteristics of a 6 MV beam in a water phantom, with emphasis on the contribution of scattered photons and charged particles to out-of-field radiation, in order to optimize PD management. We further analyzed the behavior of PD versus depth using beam characteristics determined at the surface and different depths. For the stated goal, the Monte Carlo model of the treatment head of a Siemens Oncor Impression linear accelerator was developed and commissioned.

2. Material and methods

The EGSnrc user code, BEAMnrc, (Rogers et al., 1995) was used to simulate the treatment head. To provide the characterization of the initial electron beam, some fine tuning of different parameters for the electron beam source and treatment head components was done in order to match the Monte Carlo calculated dose distributions with the measured ones. Dose calculations were performed by the EGSnrc user code, DOSXYZnrc (Walters et al., 2006). The BEAM data processor (BEAMDP), was used to analyze the phase-space files (Ma and Rogers, 2006). BEAMDP is used as a general-purpose BEAM utility program to derive energy, planar fluence, mean energy, angular distributions from existing phase-space data files generated by BEAMnrc.

2.1. Linac simulation

The detailed geometry and composition of the treatment head components were obtained from the manufacturer. Simulations were performed using a 6 MV photon beam. The incident electron beam was assumed to be monoenergetic and monodirectional, and its radial intensity distribution was considered to be Gaussian (Aljarrah et al., 2006). Therefore, an elliptical beam with a Gaussian distribution was used. The first estimation of mean energy and of the full-width-at-half-maximum (FWHM) of the intensity distribution of the electron beam was based on nominal data from the manufacturer i.e., a mono-energetic 6 MeV and Gaussian intensity distribution with a 2 mm FWHM. Field sizes were defined at the isocenter, located at 1.0 m from the source (upper face of the target).

The component modules used in the simulations were: SLABS for target, FLATFILT for flattening filter, CHAMBER for ionizing chamber, MIRROR for mirror, JAWS for secondary collimators (Y1 and Y2) and MLC for MLC. Simulations were performed for two field sizes, $10\times10\ cm^2$ and $40\times40\ cm^2$, for which 5×10^8 and 10^8 histories/particles were used, respectively. For model commissioning, the phase space data of the particles exiting the treatment head were collected at a scoring plane located at 431 mm from the source (upper face of the target).

To speed up the simulations, directional bremsstrahlung splitting (DBS) was used as variance reduction techniques. Simulation parameters were selected as follows: bremsstrahlung splitting number was 1000, lower charged particle cutoff energy, ECUT, was 0.7 MeV and the lower photon cutoff energy, PCUT, was 0.01 MeV. The energy loss per transport step of the electron, ESTEPE, was controlled by PRESTA (Parameter Reduced Electron-Step Transport Algorithm) (Bielajew and Rogers, 1987).

2.2. Dose calculations

Using the scored phase space data, the dose distribution in water phantom was calculated by DOSXYZnrc. The calculated data include central axis depth dose distributions for a field size of $10\times10\ cm^2$ and lateral dose distributions for the linac's largest field size, $40\times40\ cm^2$,at depth of 10 cm (Aljarrah et al., 2006). A $0.8\times0.8\times0.3\ m^3$ water phantom was used to incorporate sufficient backscatter material from the bottom and walls of the phantom. Depending on the required spatial resolution, the size of the phantom's voxels (xyz) for the depth–dose calculations along the central axis varied between $20\times20\times2\ mm^3$ (in the build-up region) and $20\times20\times10\ mm^3$ and for the profile calculations between $1\times20\times5\ mm^3$ (in the penumbra region) and $20\times20\times5\ mm^3$ (in out-of-field).

The physical parameters of the original electron beam that may influence the dose profile and central-axis PDD curve are beam energy, beam spot size and distance from the source (Lin et al., 2001; Sheikh-Bagheri and Rogers, 2001). The off-axis factors were found to be very sensitive to the mean energy of the electron beam, the FWHM of its intensity distribution, its angle of incidence, the dimensions of the upper opening of the primary collimator, the material of the flattening filter and its density (Sheikh-Bagheri and Rogers, 2001). No energy spread for electron beam was considered because this parameter showed no considerable influence on beam profile or depth dose curves (Sheikh-Bagheri and Rogers, 2002; Tzedakis et al., 2004). The mean energy and the FWHM of the incident electron beam intensity distributions were derived by matching calculated percentage depth–dose curves and off-axis factors with measured data.

2.3. Dose measurements

Dose distribution measurements were done with an automatic water phantom (Medphysto mc2, mp3, PTW, Germany) and two $0.12\ cm^3$ PTW ionization chambers ($N_{D,W,\ Co60}$, the calibration factor in terms of absorbed dose to water obtained from IAEA/WHO SSDL network=5.31 cGy/nC) as reference and dose chambers. Measurements were performed at a source-to-surface distance (SSD) of 1.0 m. A correction for the displacement of the measurement point of the chamber towards the phantom surface was applied. Measurements were performed with 1 mm resolution for both PDD curves and beam profiles. The overall measurement uncertainty, including 1.5% chamber calibration uncertainty, was 2.5%. The sources of experimental uncertainty were inaccuracy in chamber positioning of up to 1 mm and short-term fluctuations of the chamber, electrometer, air pressure and temperature during each measurement (Khan, 2003; International Atomic Energy Agency (IAEA), 2000). The uncertainties were within the resolution of the symbols used in the plots.

Absorbed dose determination was performed according to the recommendations of IAEA's TRS-398 protocol (International Atomic Energy Agency (IAEA), 2000). Calculation of absorbed dose requires knowledge of the average energy of the photon spectrum at the point of measurement. The PD was measured in the peripheral regions of the fields, where the average energy of the photon spectrum cannot be measured accurately. Fortunately the parameters in the dose calculation protocol vary by less than 1% for a 6 MV photon spectrum and also the response of an ion chamber is quite flat over this energy range (International Atomic Energy Agency (IAEA), 2000; Podgorsak et al., 1999).

3. Results and discussion

3.1. Monte Carlo model commissioning

The mean energy of the electron beam for 6 MV photons was determined to be 6.7 MeV with an uncertainty of 0.1 MeV, as derived from the 0.1 MeV resolution of electron beam energy in

the BEAMnrc code. This value was obtained by comparing the calculated and measured PDD for the 10×10 cm^2 field size. This comparison is shown in Fig. 1. The local differences between measurements and calculations are less than 2% except for the surface dose. Since the statistical uncertainty was less than 2% at depth of maximum dose (dmax), it was possible to normalize the absorbed dose values to dmax for the PDD distribution.

Beam profiles, calculated and measured at depth of 10 cm for a field of 40×40 cm^2 are shown in Fig. 2. To compare the profiles, the percentage difference for each point was defined as the percentage ratio between calculated and measured values. For each region, the percentage difference was evaluated against those recommended by Venselaar et al. (2001) as criteria for the acceptance of calculation results in a water phantom. The results of the comparison of the calculated and measured beam profile together with statistical uncertainty of calculations are given in Table 1. The observed differences between the measurements and the calculations, other than uncertainty in the stopping power values and statistical

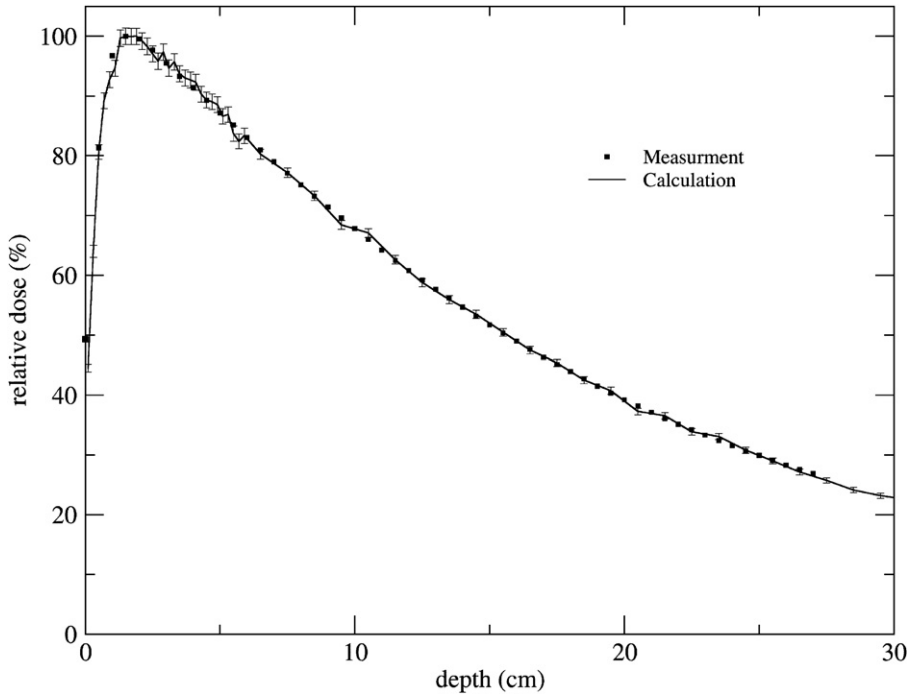

Fig. 1. Comparison of calculated and measured percent depth dose curves for 6 MV photon beam for field size of 10×10 cm^2.

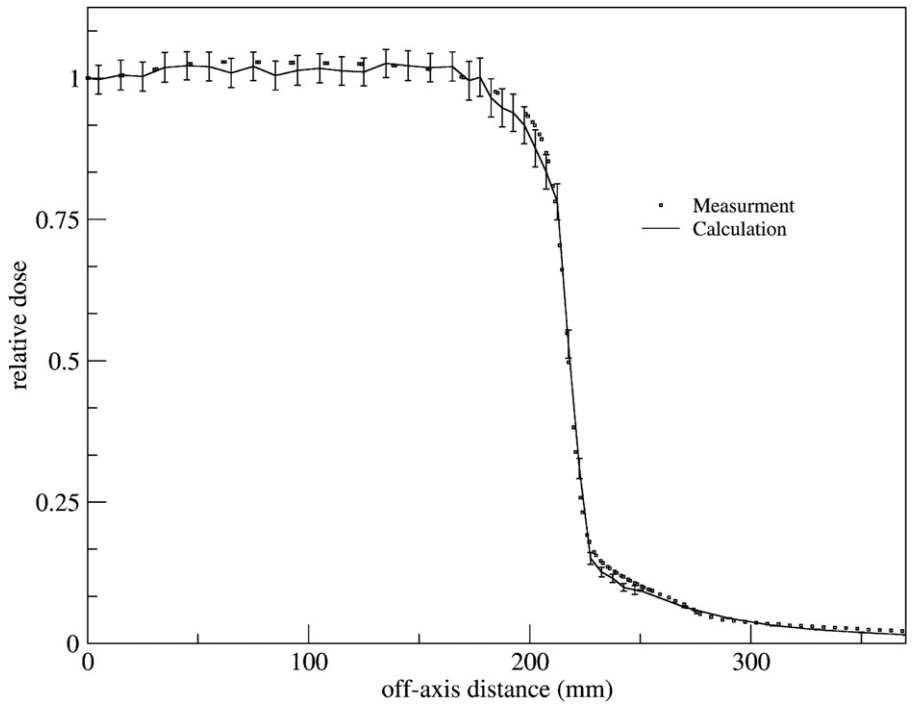

Fig. 2. Comparison of calculated and measured dose profiles, 6 MV photon beam at 10 cm depth and 40×40 cm^2 field size.

uncertainty in Monte Carlo results, may be due to fluctuations of the linac's output, depth dependency of dosimetry factors, uncertainties of the measurements and approximation in manufacturer provided information about linac components.

Table 1

Region in profile	Acceptance criteria	Statistical uncertainty (%)	Local difference (%) - (mm)
Flat (umbra)	2%	0.6–1.3	1.04%
penumbra	10%–2 mm	3.7–4	7.5%–2 mm
Out of field	30%	4–9	17%

3.2. Phase spaces analysis with BEAMDP

In order to further analyze the depth independency of PD, the behavior of beam characteristics with depth was investigated by BEAMDP. Phase space data was scored for $10\times10\,cm^2$ and $40\times40\,cm^2$ field sizes in a phantom located at SSD = 1.0 m, at the surface, and in depths of 5 and 10 cm. The phantom was simulated using three CONESTAK component modules in BEAMnrc. CONESTAK is a coaxial truncated cone surrounded by a cylindrical wall. The BEAMnrc LATCH variable was used to separate the contribution of different particles to beam characteristics at different depths and off-axis distances. This variable, associated with each particle in a simulation, is a 32-bit variable used to track the particle's history. Using this variable one records

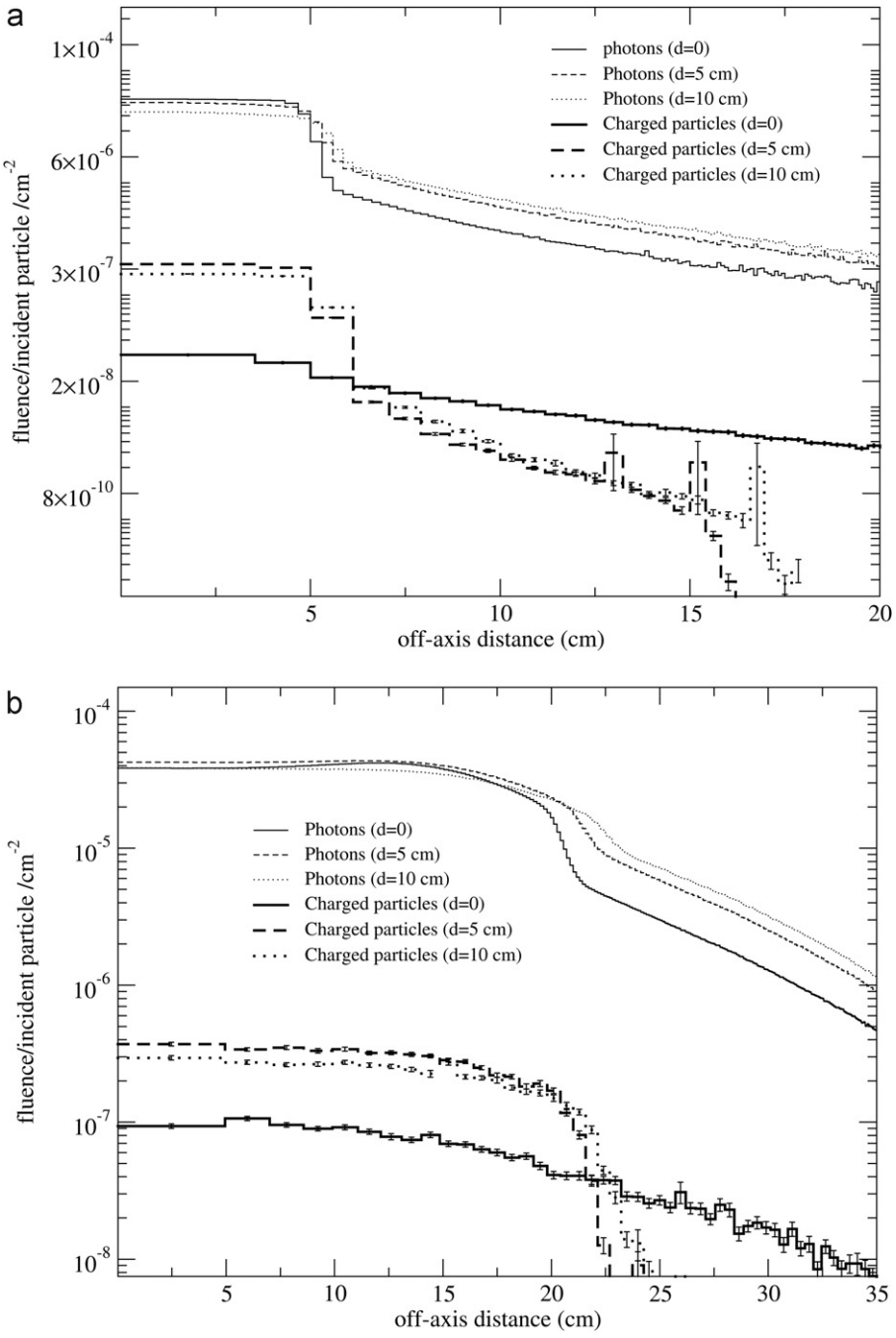

Fig. 3. Fluence of photons and charged particles as a function of distance from the central axis at phantom surface and 5 and 10 cm depths for two field (a) $10\times10\,cm^2$ and (b) $40\times40\,cm^2$, 6 MV photon beam at SSD = 1.0 m.

each particle's complete history of where a particle has been or where a particle has interacted in the beam simulation. In this work, the contribution of particles interacted and or originated in the phantom was separated from the total scored data at each depth. The origin of a photon is considered to be the region where it is created as a bremsstrahlung photon or scattered after a Compton or coherent scattering event. For a charged particle, the origin is considered to be the last non-air region it has been to before it reaches the scoring plane (Ma and Rogers, 2006).

The parameters specified for BEAMDP were as follows: 30 keV interval energy, 180angular bins, and zero and 90 degrees minimum and maximum angles, the angle between the direction of particles incident on the scoring plane and the z-axis, respectively. To derive the angular distributions, the scoring planes were as large as the corresponding field sizes and for other parameters; analysis was performed up to 0.15 m from each field's edge. The BEAMDP analysis results, including fluence profiles, energy fluence profiles, mean energy and angular distribution for photons and contaminating charged particles at different depths and different distances from the field edge, are shown in Figs. 3–6.The statistical uncertainty is often less than 0.1% and therefore not shown on the plots.

For a 10×10 cm^2 field, the photon fluence inside the field at the phantom surface ($d=0$) and at two depths in the phantom remains constant until a relatively sharp decrease at the field edge occurs (Fig. 3(a)). As the depth increases, this parameter decreases due to photon attenuation with depth. In contrast, an increase in photon fluence with depth is seen outside the field,

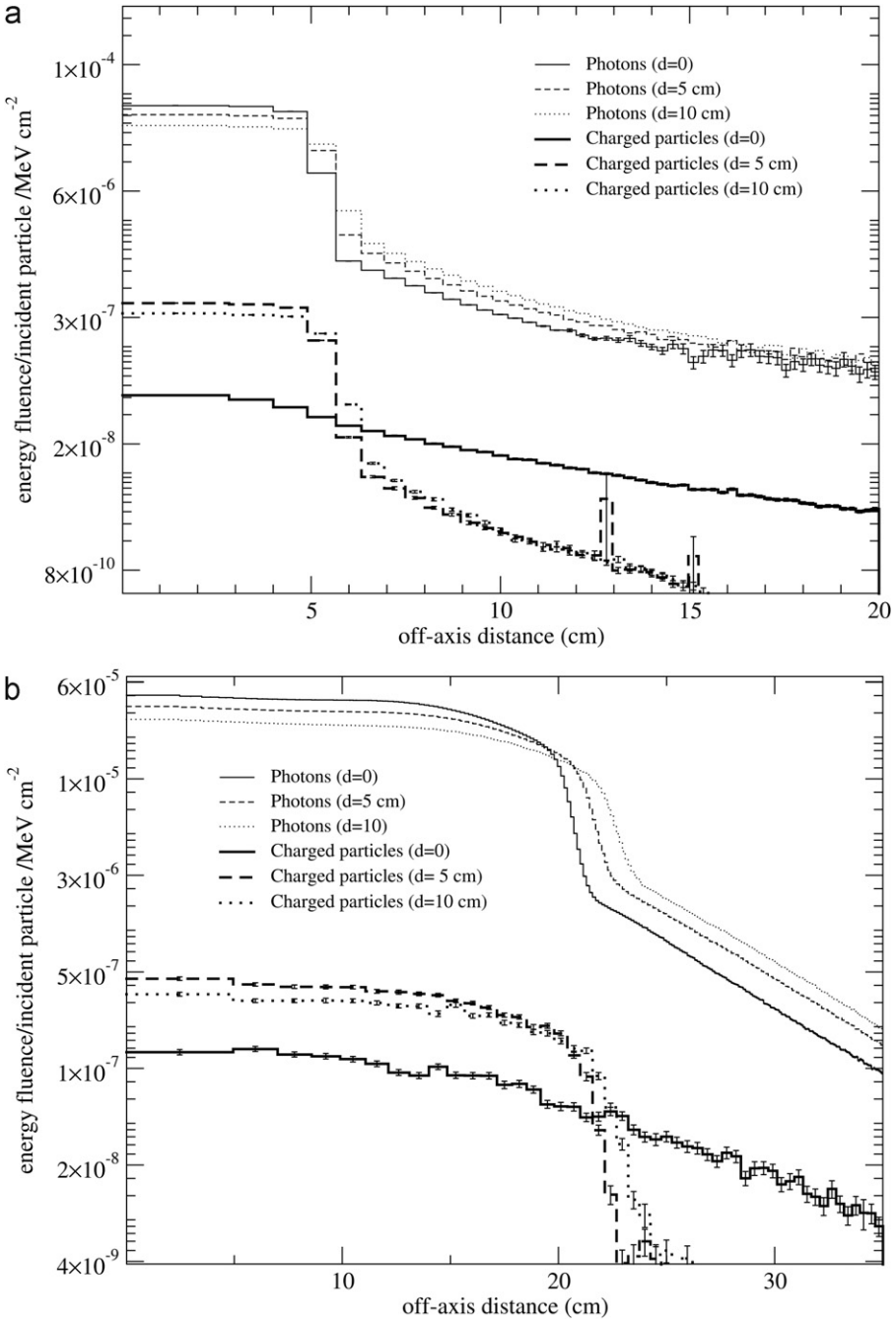

Fig. 4. The energy fluence of photons and charged particles as a function of distance from the central axis at phantom surface and 5 and 10 cm depths for two field (a) 10×10 cm^2 and (b) 40×40 cm^2, 6 MV photon beam at SSD=1.0 m.

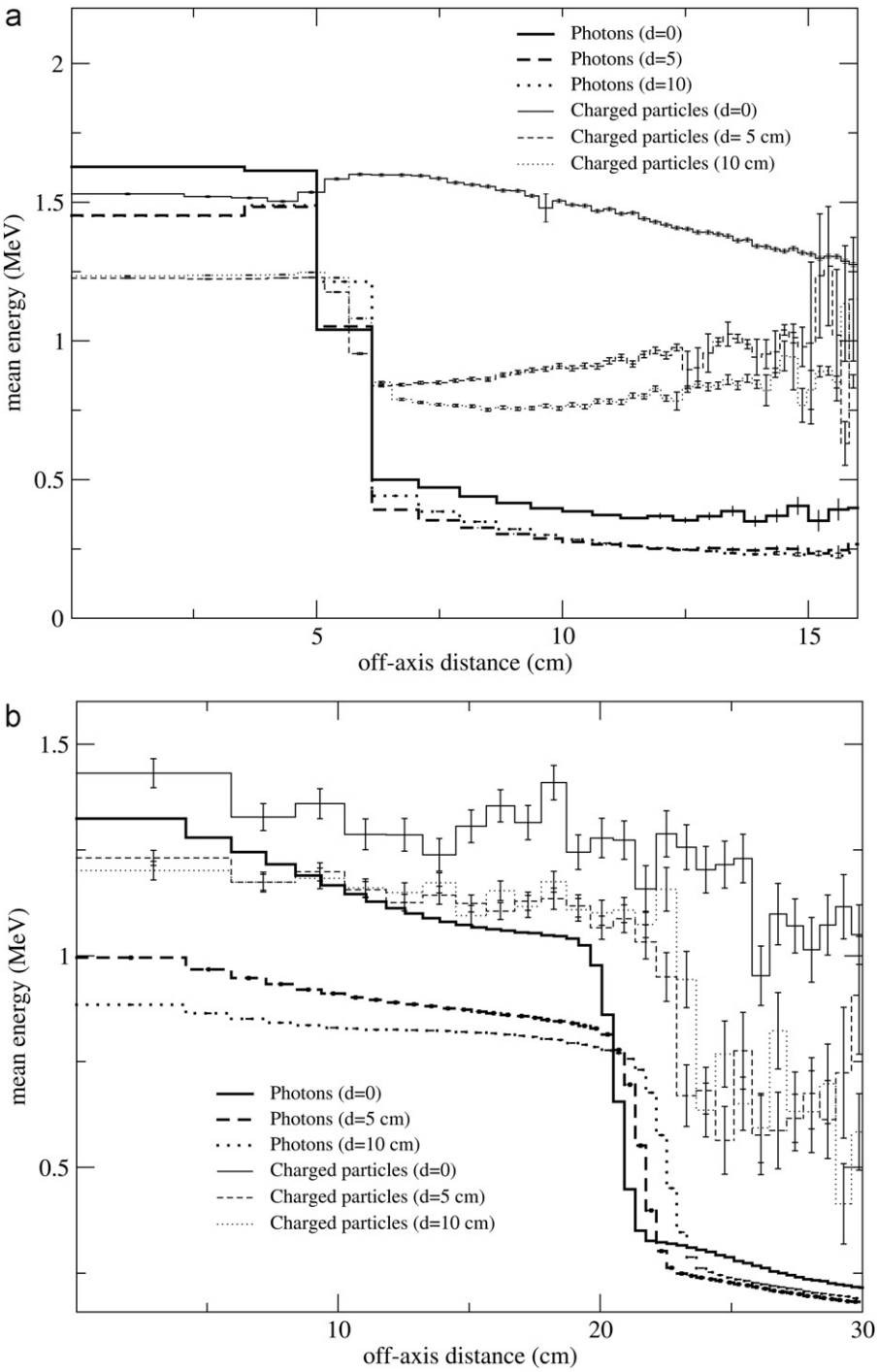

Fig. 5. The mean energies of photons and charged particles as a function of off axis distance at the phantom surface and 5 and 10 cm depths for two field (a) 10×10 cm^2 and (b) 40×40 cm^2, 6 MV photon beam at SSD = 1.0 m.

due to beam divergence and as later shown due to the increase in phantom scatter fluence with depth (Fig. 7). Inside the field however, the charged particle fluence first increases with depth and then decreases due to photon attenuation. A sharp decrease at the field edge is also observed for the charged particle fluence at 5 and 10 cm depths. However, their fluence at the surface shows a more gradual fall off. The same distribution for photon and charged particle fluence versus depth and distance from central axis is seen for 40×40 cm^2 field size (Fig. 3(b)).

The energy fluence profiles of photons and charged particles for both field sizes 10×10 cm^2 and 40×40 cm^2 (Fig. 4), show a depth dependence similar to the fluence profiles. However, for 40×40 cm^2, the energy fluence profiles for photons show the effect of beam hardening created by the flattening filter at the center of the field.

The spatial distribution of the mean energy of photons at the surface is rather flat inside the field and decreases slightly towards the field edge where sharp drop occurs as shown in Fig. 5(a) for the 10×10 cm^2 field size. Whereas, the mean energy profiles inside the phantom showed an increase toward the field's boundary. Along the beam axis, the mean energy was reduced from 1.63 MeV at the surface to an identical energy of 1.44 MeV at both 5 and 10 cm depth. The wider distribution of mean energy at 10 cm depth around the beam boundary is related to beam divergence with depth. The same depth independency is present

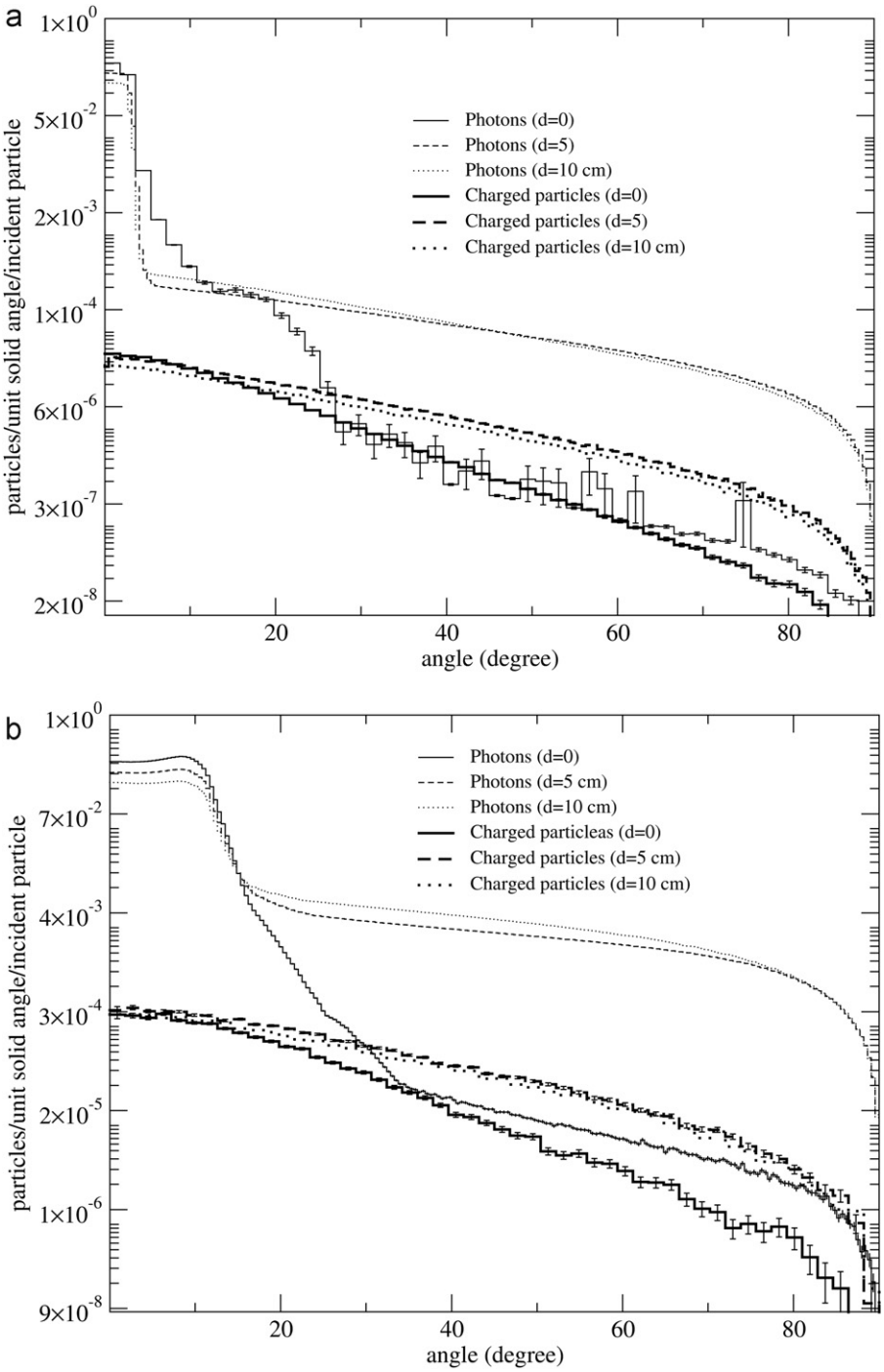

Fig. 6. The angular distribution of photons and charged particles as a function of distance from the central axis at phantom surface and 5 and 10 cm depths for two field (a) 10×10 cm^2 and (b) 40×40 cm^2, 6 MV photon beam at SSD = 1.0 m.

for the mean energy of charged particles, where the mean energy along the beam axis changed from 1.53 MeV at the surface to a constant value of 1.23 at both depths. However, at the surface, the profile showed a slight increase outside and near the border.

A similar depth dependency and sharp drop outside the field were notable in the mean energy profiles of photons and charged particles for 40×40 cm^2 field. For this field size, the mean energy profiles for photons showed a maximum on the central axis at all depths and a change in gradient as depth increased, i.e., 28% at $d=0$, 20% at $d=5$ and 10% at $d=10$. Along the beam axis, the mean energy of photons decreased from 1.33 MeV on the surface to 0.99 MeV at 5 cm depth and 0.89 MeV at 10 cm. The mean energy of the charged particles also decreased from 1.44 MeV at the surface to 1.22 MeV at 5 cm and to 1.19 MeV at 10 cm. For both field sizes, the mean energy of photons and charged particles inside and outside the field was less than one third of the nominal beam energy. Also the mean energy distribution of photons and charged particles in out-of-field regions were nearly independent of depth. Therefore, for the range of peripheral mean energy variations seen in this study, the ionization chamber energy correction factor remains constant (International Atomic Energy Agency, 2000). The ionization chamber energy correction factor is used to correct the dose to water calibration factor from a reference beam to the actual user's quality. Thus, for absolute

peripheral dose measurements, a single energy correction factor can be used, independent of depth and distance from the field's edge. For the same reason, variation of air to water stopping power ratio with electron energy for the range of peripheral mean energy variations seen, is quiet minimal. Therefore, depth ionization distributions measured with an ionization chamber in out-of-field may be used directly to give depth dose distributions.

Fig. 6(a), (b) present the angular distributions of photons and charged particles at 0, 5 and 10 cm depths for the 10×10 cm^2 and 40×40 cm^2 field sizes. For both field sizes, photons showed narrow angular distributions both at the surface and with depth, although there was a wider distribution for the larger field. However, charged particles showed a wider angular distribution. This distribution changed with field size and stayed almost constant with depth.

In order to further analyze the contribution of phantom scatter to out-of-field radiation, the LATCH variable was used and the associated results are illustrated in Figs. 7–10. The statistical uncertainty is often less than 0.1% and therefore not shown on the plots.

The fluence profiles were analyzed to estimate the abundance of different particles versus depth and distance from central axis. As shown in Fig. 7, for photons interacting with phantom (phantom photons), the fluence increases with depth and suffers a slower drop at the field border, in contrast to the fluence of incident photons (shown in Fig. 3). Within the field boundaries and in each depth, the number of phantom photons was about 2% of the total incident photons. Whereas, nearly all of phantom charged particles were originated in the phantom. In the phantom however, the majority of charged particles in out-of-field regions

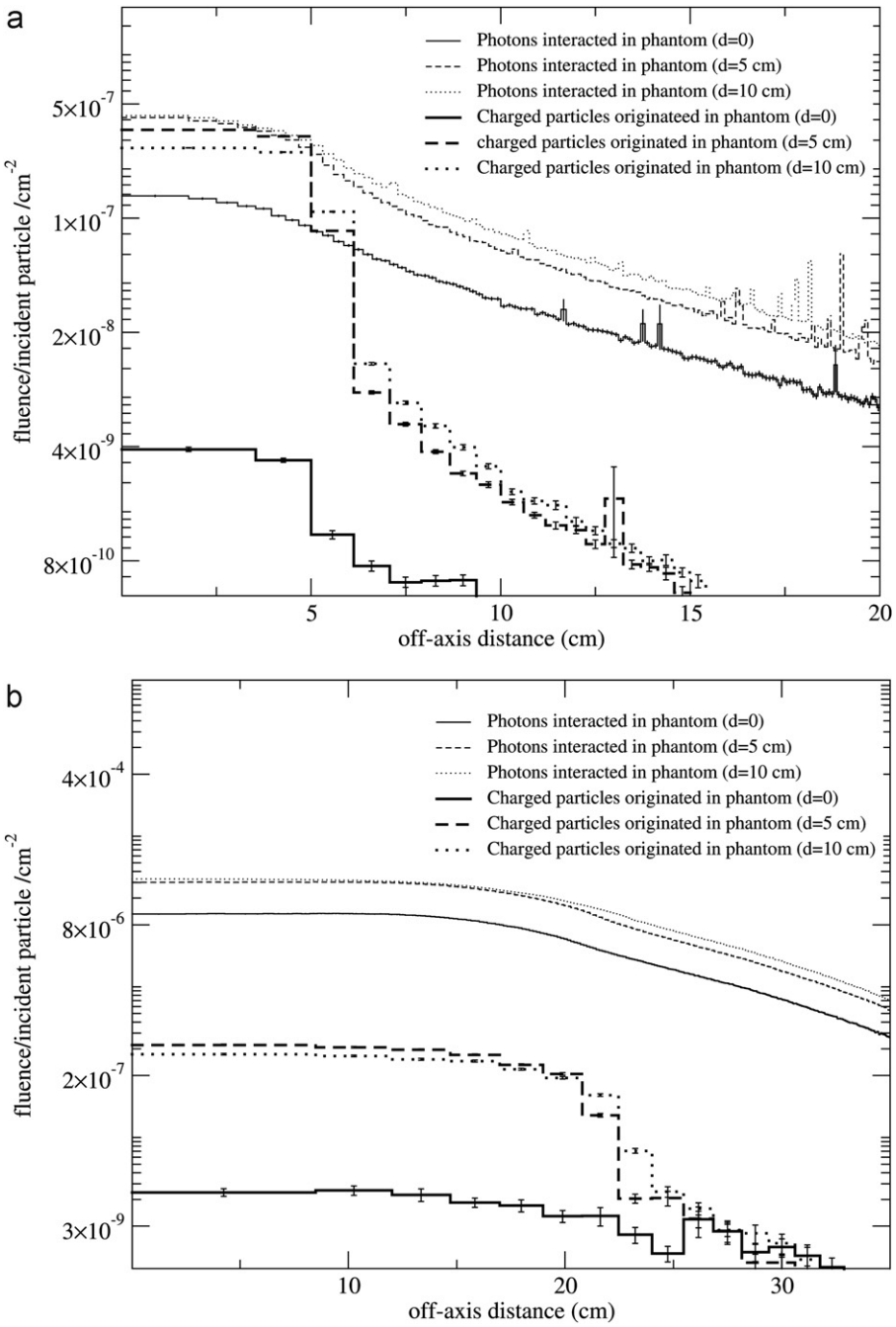

Fig. 7. Fluence of photons and charged particles those interacted and originated in phantom as a function of distance from the central axis at phantom surface and 5 and 10 cm depths for two field (a) 10×10 cm^2 and (b) 40×40 cm^2, 6 MV photon beam at SSD = 1.0 m.

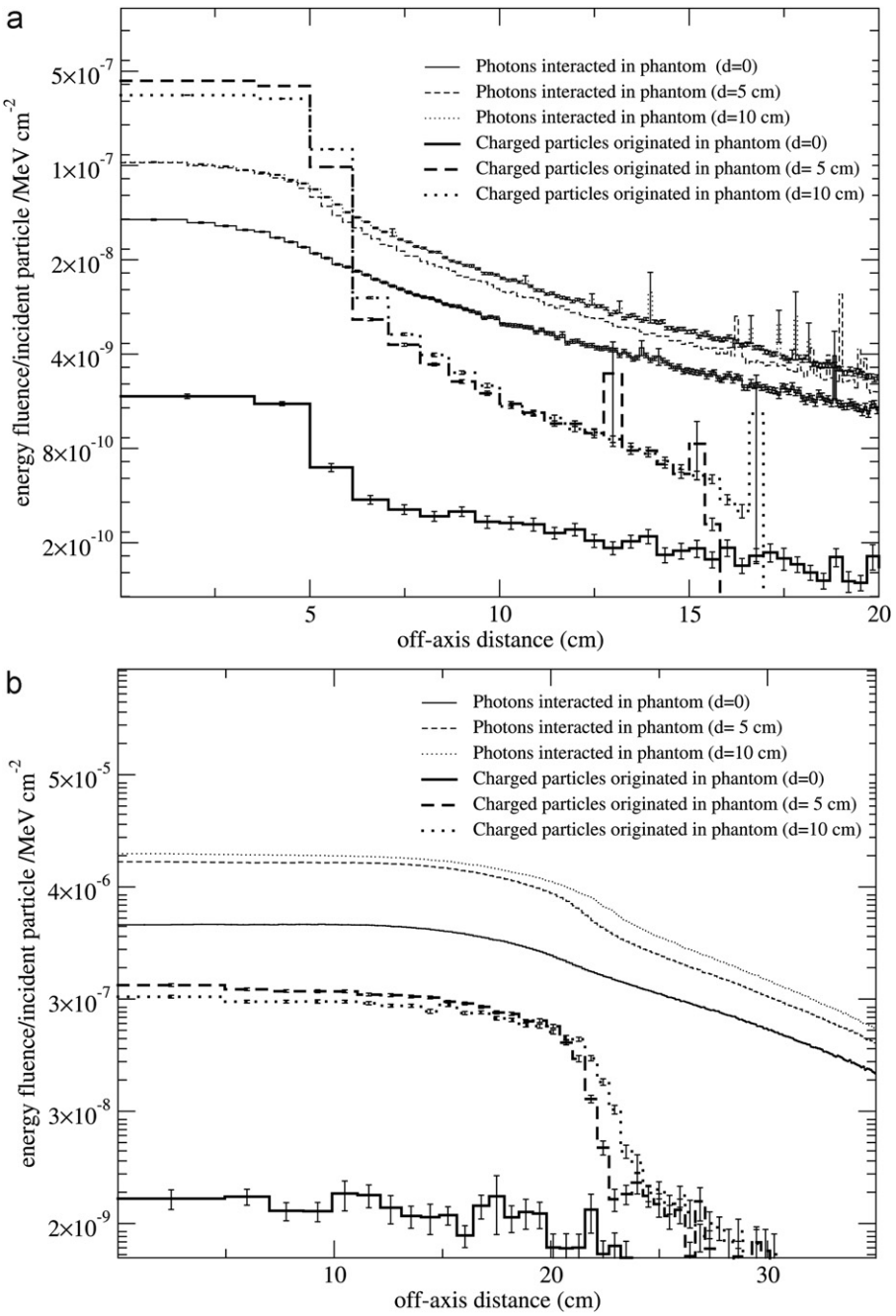

Fig. 8. The energy fluence profiles of photons and charged particles those interacted and originated in phantom as a function of distance from the central axis at phantom surface and 5 and 10 cm depths for two field (a) 10×10 cm^2 and (b) 40×40 cm^2, 6 MV photon beam at SSD = 1.0 m.

were originated in the irradiated volume in contrast to those produced due to interaction of head leakage and head scatter photons with phantom. This finding confirms that using an external shield in out-of-field regions will not reduce the dose due to particles scattered from the irradiated volume. Considering this fact, one may design an effective external shield for out-of-field organs with minimum thickness.

In Fig. 8, for both particle types and each field size, the same pattern of dependency with depth observed in Fig. 7 is seen for the spatial distribution of energy fluence. In Fig. 9, the mean energy distribution of phantom photons and phantom charged particles is shown. As shown in Fig. 9(a), the mean energy distribution of phantom photons did not change with depth and remained constant inside and outside the 10×10 cm^2 field. For this field, a larger mean energy value for phantom charged particles relative to phantom photons is shown. However, for the 40×40 cm^2, the mean energy decreased outside the field's border. For phantom charged particles, the mean energy at the surface remained constant in and out-of-field and increased at depth relative to the surface for both field sizes. A sharp reduction in the mean energy was observed for both depths and field sizes.

In Fig. 10, phantom photons and charged particles showed similar angular distributions irrespective of depth and field size. However, for the 40×40 cm^2 field size the abundance of phantom photons scattered in wide angles was greater than charged particles. Therefore, probability of phantom photons contamination in out-of-field regions is greater than that for charged particles.

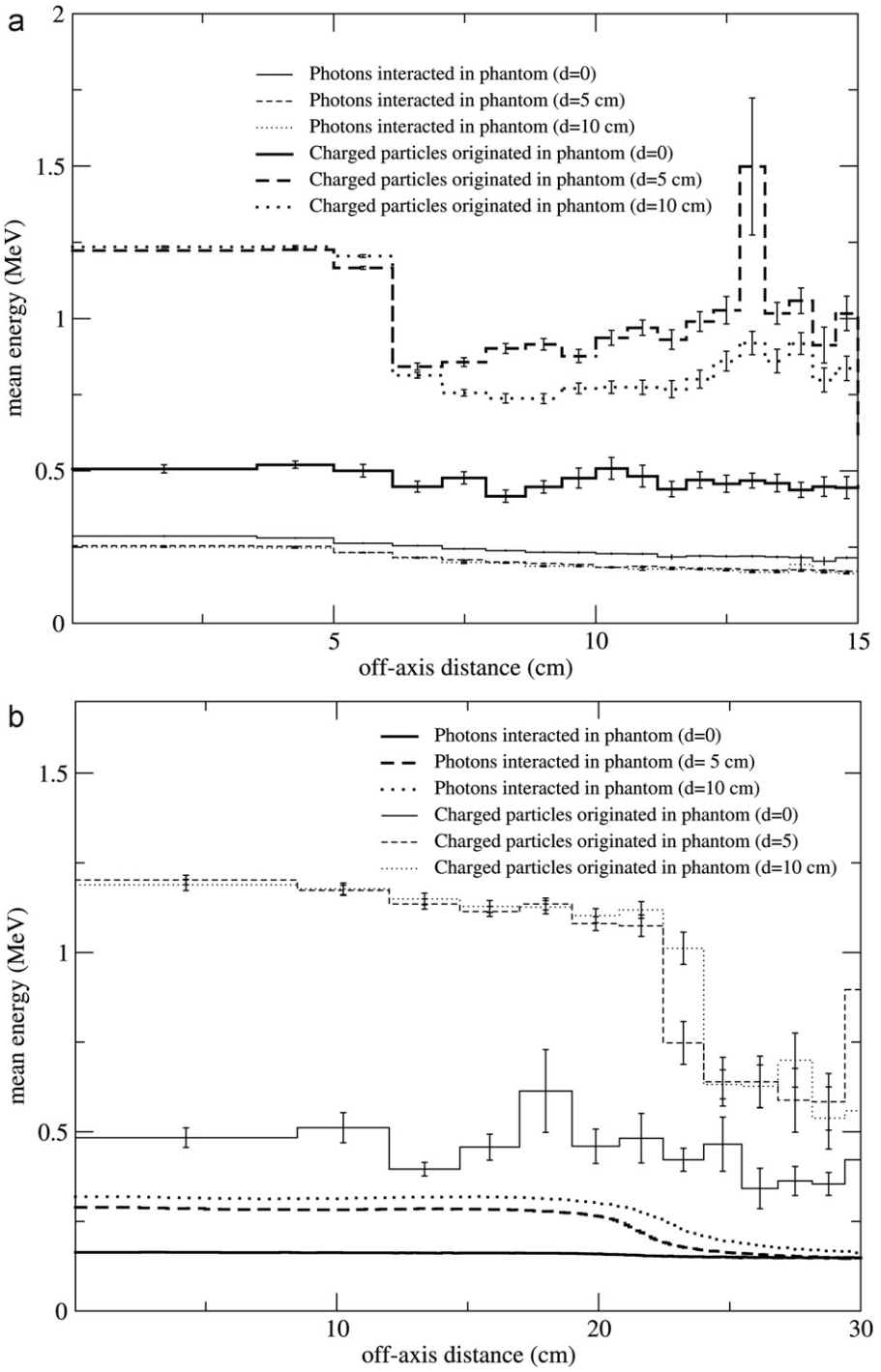

Fig. 9. The mean energy distribution of photons and charged particles those interacted and originated in phantom as a function of distance from the central axis at phantom surface and 5 and 10 cm depths for two fields (a) $10 \times 10\ cm^2$ and (b) $40 \times 40\ cm^2$, 6 MV photon beam at SSD = 1.0 m.

3.3. Out-of-field dose calculations

In order to investigate the behavior of out-of-field dose with depth, the depth dose curves were calculated at four different distances; 2, 5, 7 and 10 cm from the edge of a $10 \times 10\ cm^2$ field (Fig. 11). Calculations were done in water phantom, irradiated with 6 MV photon beam at SSD = 1.0 m. These results show that PD, as a percentage of maximum dose along central axis, decreased from about 40% at the field border to 6% in other distances from the edges of the field, respectively. Also it can be seen that PD was independent of depth at all distances.

In this study, it was shown that incident photon energy fluence remains constant with depth in out-of-field regions. Therefore, in this region the attenuation and scattering of photons at different depths was negligible and charged particle equilibrium (CPE) exists. Under CPE, dose is equal to collision kerma (Kcol). The ratio of Kcol at two depths is proportional to the ratio of product of the energy fluence and the mass attenuation coefficient at the corresponding depths. It was also shown that the incident photon mean energy remained constant with depth in out-of-field regions. Therefore, for these photons, the ratio of average attenuation coefficients at two depths is unity and the ratio of Kcol at two

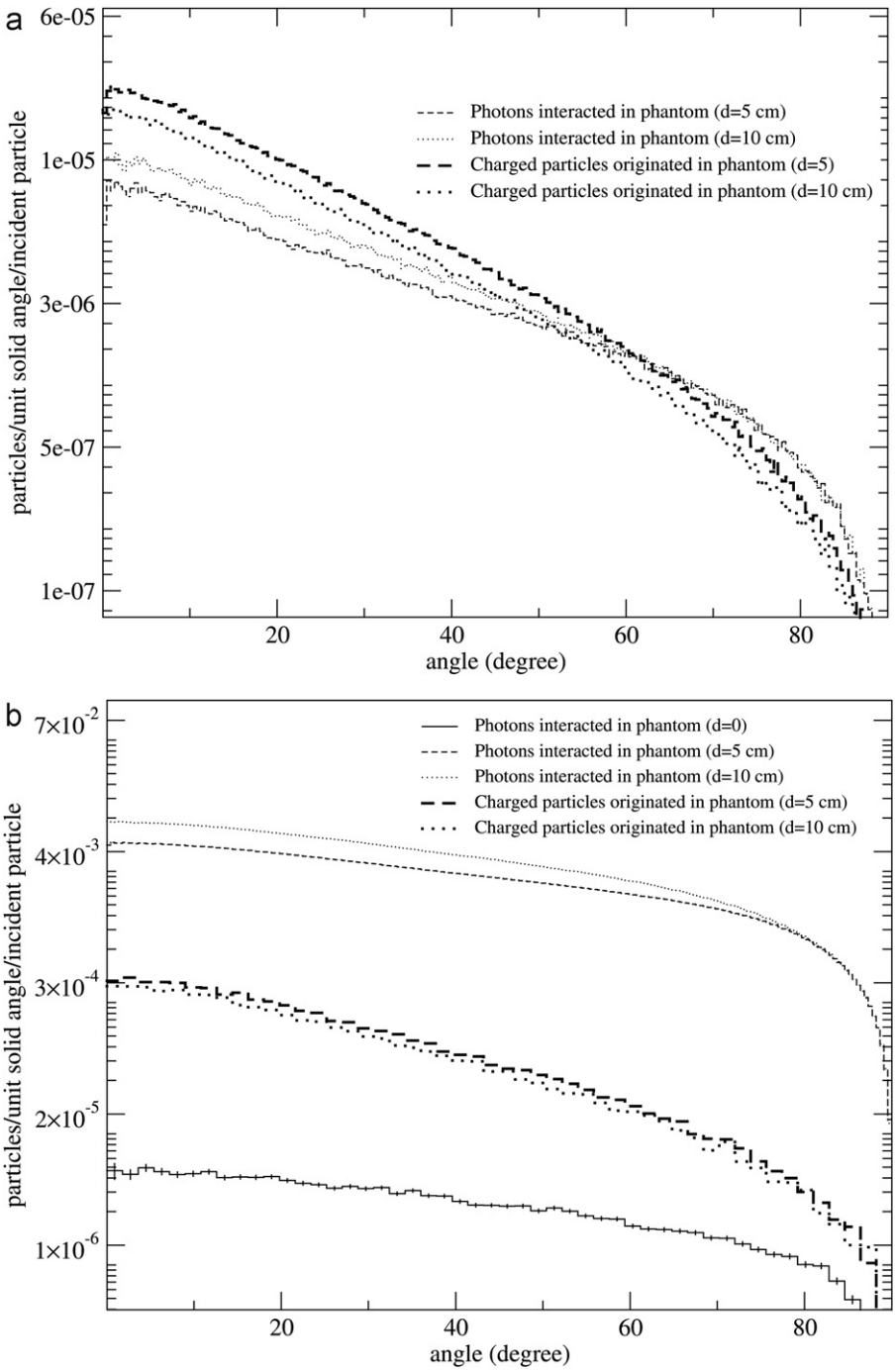

Fig. 10. The angular distribution of photons and charged particles those interacted and originated in phantom as a function of distance from the central axis at phantom surface and 5 and 10 cm depths for two fields (a) $10 \times 10\ cm^2$ and (b) $40 \times 40\ cm^2$, 6 MV photon beam at SSD = 1.0 m.

depths is proportional to the ratio of the energy fluence at the corresponding depths outside the field boundary. Therefore, outside the field boundary, Kcol remains constant with depth and it can be concluded that PD is independent of depth. In vicinity of the field border, however, a larger variation of PD with depth was seen.

4. Conclusion

Monte Carlo simulations were conducted to investigate the characteristics of particles originated in the irradiated volume and their contribution to out-of-field radiation. A Siemens Oncor Impression treatment head was modelled for a 6 MV photon beam using BEAMnrc user code. The calculated percent depth dose and dose profile plots show good agreement with measurements. Using the developed model, energy and spatial distributions for the incident particles and the scattered particles created in phantom were calculated. All data are presented for field sizes of $10 \times 10\ cm^2$ and $40 \times 40\ cm^2$, at the surface and at the two depths in the phantom.

At the surface, inside and outside the field, fluence of charged particles created in the phantom was negligible compared to the incident charged particle fluence. In the phantom however, the majority of charged particle in out-of-field regions were originated in the irradiated volume in contrast to those produced due to interaction of head leakage and head scatter photons with

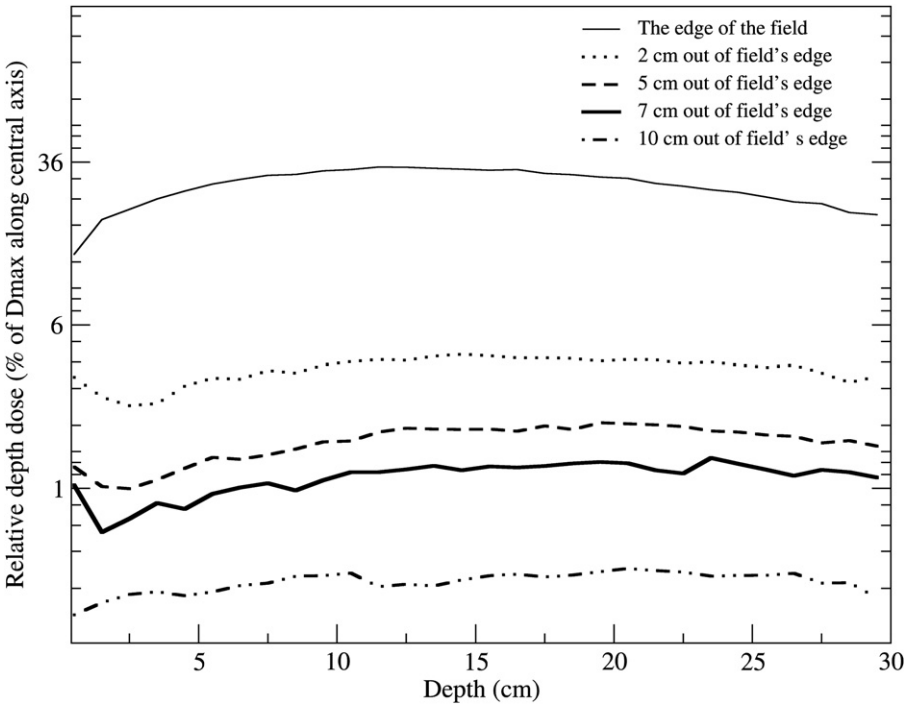

Fig. 11. Relative dose values calculated from the water surface to 30 cm depth at the edge of the field and 2, 5, 7 and 10 cm from the edge of a $10 \times 10\ cm^2$ field.

phantom. This finding confirms that using an external shield in out-of-field regions will not reduce the dose due to particles scattered from the irradiated volume.

In out-of-field regions, the mean energy profiles for photons and charged particles remained nearly constant with depth and lateral distance. These results can be used for determination of conversion factors used in dosimetry when converting detector reading to dose. For example, when measuring relative peripheral depth dose distributions using an ionization chamber, the ratio of ionization at each depth to ionization at depth of maximum will be equal to depth dose ratios. Therefore, conversion of depth ionization distribution to depth dose distribution is not needed. Also, for the range of peripheral mean energy variations shown in this study, the energy correction factor for correction of dose to water calibration factor from the reference quality to the user's energy is constant. Therefore, for absolute peripheral dose measurements, a single energy correction factor can be used, independent of depth and distance from the field's edge.

Finally, it was shown that incident photon energy fluence remained constant with depth in out-of-field regions. Using this finding, the charged particle equilibrium concept and relationship of collision kerma and dose, the fact that peripheral dose is independent of depth was justified.

Acknowledgments

The authors are grateful to Dr. Joanna Cygler for useful comments on the manuscript. The authors wish to acknowledge support from the department of radiotherapy of Milad Hospital, Isfahan, Iran. The authors would also like to thank Dr. Amouheidari for providing support during this research and Shahram Monadi for suppling some measured data.

References

Aljarrah, K., Sharp, G.C., Neicu, T., Jiang, S.B., 2006. Determination of the initial beamparameters in Monte Carlo linac simulation. Med. Phys. 33, 850–858.

Bielajew, A.F., Rogers, D.W.O., 1987. PRESTA: the parameter reduced electron-step transport algorithm for electron Monte Carlo transport. Nucl. Instrum. Methods Phys. Res., Sect. B. 18, 165–181.

Chaney, E.L., Cullip, T.J., 1994. A Monte Carlo study of accelerator head scatter. Med. Phys. 21, 1383–1390.

Chofor, N., Harder, D., Ruhmann, A., Willborn, K.C., Wiezorek, T., Poppe, B., 2010. Experimental study on photon-beam peripheral doses, their components and some possibilities for their reduction. Phys. Med. Biol. 55, 4011–4027.

Chofor, N., Harder, D., Willborn, K.C., Poppe, B., 2012. Internal scatter, the unavoidable major component of the peripheral dose in photon-beam radiotherapy. Phys. Med. Biol. 57, 1733–1743.

Deng, J., Jiang, S.B., Kapur, A., Li, J., Pawliki, T., Ma, C.M., 2000. Photon beam characterization and modeling for Monte Carlo treatment planning. Phys. Med. Biol. 45, 411–427.

Ding, G.X., 2002. Energy spectra, angular spread, fluence profiles and dose distributions of 6 and 18 MV photon beams: results of Monte Carlo simulations for a Varian 2100EX accelerator. Phys. Med. Biol. 47, 1025–1046.

Jiang, S.B., Boyer, A.L., Ma, C.M., 2001. Modeling the extrafocal radiation and monitor chamber backscatter for photon beam dose calculation. Med. Phys. 28, 55–66.

Khan, F.M., 2003. The Physics of Radiation Therapy, fourth ed. Lippincott Williams & Wilkins, Philadelphia.

Kim, H.K., Han, S.J., Kim, J.L., Kim, B.H., Chang, S.Y., Lee, J.K., 2006. Monte Carlo simulation of the photon beam characteristics from medical linear accelerators. Radiat. Prot. Dosim. 119, 510–513.

Kry, S., Titt, U., Ponisch, F., Followill, D., Vassiliev, O.N., White, R.A., Mohan, R., Salehpoura, M., 2007. A Monte Carlo model for out-of-field dose calculating from high-energy photon therapy. Med. Phys. 34, 3489–3499.

Kry, S., Titt, U., Ponisch, F., Followill, D., Vassiliev, O.N., White, R.A., Mohan, R., Salehpoura, M., 2006. A Monte Carlo model for calculating out-of-field dose from a Varian 6 MV beam. Med. Phys. 33, 4405–4413.

Lin, S.Y., Chua, T.C., Lin, J.P., 2001. Monte Carlo simulation of a clinical linear accelerator. Appl. Radiat. Isot. 55, 759–765.

Lovelock, D.M.J., Chui, C.S., Mohan, R., 1995. A Monte Carlo model of photon beams used in radiation therapy. Med. Phys. 22, 1387–1394.

Ma, C.M., Rogers, D.W.O., 2006. BEAMDP as a General-Purpose Utility NRC Report PIRS 09 rev A.

Mohan, R., Chui, C., 1985. Energy and angular distributions of photons from medical linear accelerators. Med. Phys. 12, 592–597.

Podgorsak, M., Meiler, R.J., Kowal, H., Kishel, S.P., Orner, J.B., 1999. Technical management of a pregnant patient undergoing radiation therapy to the head and neck. Med. Dosim. 24, 121–128.

Rogers, D.W.O., Faddegon, B.A., Ding, G.X., Ma, C.M., We, J., Mackie, T.R., 1995. BEAM: a Monte Carlo code to simulate radiotherapy treatment units. Med. Phys. 22, 503–524.

Sheikh-Bagheri, D., Rogers, D.W.O., 2002. Monte Carlo calculation of nine megavoltage photon beam spectra using the BEAM code. Med. Phys. 29, 391–402.

Sheikh-Bagheri, D., Rogers, D.W.O., 2001. Sensitivity of megavoltage photon beam Monte Carlo simulations to electron beam and other parameters. Med. Phys. 29, 379–390.

Stoval, M., Blackwell, C.R., Cundiff, J., Novack, D.H., Palta, J.R., Wagner, L.K., Webster, E.W., Shalek, R.J., 1995. Fetal dose from radiotherapy with photon beams: report of AAPM radiation therapy task group no. 36. Med. Phys. 22, 63–82.

Tzedakis, A., Damilakis, J.E., Mazonakis, M., Stratakis, J., Varveris, H., Gourtsoyiannis, V., 2004. Influenciess of initial electron beam parameters on Monte Carlo calculated absorbed dose distributions for radiotherapy photon beams. Med. Phys. 31, 907–913.

Venselaar, J., Welleweerd, H., Mijnheer, B., 2001. Tolerances for the accuracy of photon beam dose calculations of treatment planning systems. Radiother. Oncol. 60, 191–201.

Walters, B., Kawrakow, I. Rogers, D.W.O., 2006. DOSXYZnrc Users Manual NRCC Report PIRS-794revB.

International Atomic Energy Agency, 2000. Absorbed Dose Determination in External Beam Radiotherapy. Technical Report Series No. 398. Vienna.